Synthesis and Characterization of a Tetradentate Bispidine-based Ligand and its Zinc(II) Complex

Matteo Mori,[a] Edoardo Fumagalli,[a,c] Carlo Castellano,[b] Andrea Tresoldi,[a] Alessandro Sacchetti[c] and Fiorella Meneghetti[a,*]

[a]*Department of Pharmaceutical Sciences, University of Milan, Via L. Mangiagalli 25, 20133 Milano, Italy.*
[b]*Department of Chemistry, University of Milan, Via C. Golgi 19, 20133 Milano, Italy.*
[c]*Department of Chemistry, Materials and Chemical Engineering "Giulio Natta", Polytechnic University of Milan, Piazza Leonardo da Vinci 32, 20133 Milano, Italy.*

Keywords

Coordination chemistry; bispidine; X-ray diffraction; Hirshfeld surface analysis; NMR titration; DFT.

Highlights

- A tetradentate diol-bispidine-based ligand and its metal complex with Zn(II) were efficiently synthesized.
- X-ray analysis defined the chair-chair (**cc**) conformation of the bispidine core.
- In the crystal structure, the metal center exhibited a distorted square pyramid coordination geometry.
- The theoretical conformation of the complex agreed with the results of the solid-state analysis.
- NMR titration studies were employed to follow the formation of the complex in solution and identify the correct stoichiometry.

Abstract

The efficient synthesis of a tetradentate diol-bispidine-based ligand and its metal complex with Zn(II) is here reported. The single-crystal X-ray diffraction (SC-XRD) analysis of the Zn(II) complex allowed the characterization of the coordination sphere around the cation as a distorted square pyramid and confirmed that the bispidine core was in a chair-chair (**cc**) conformation. This finding agreed with the theoretical analysis. The structural data demonstrated the influence of the ligand conformation on the coordination mechanism, confirming that the **cc** geometry of the bispidine core is a key factor to form a stable complex. Hirshfeld surface and two-dimensional fingerprint analysis showed that hydrogen bonds (O···H) and van der Waals interactions constituted the major contribution to the intermolecular forces, with O···H/H···O and H···H contacts accounting for 39.8% and 38.8% of the surface, respectively. NMR titration experiments provided information on the formation mechanism of the complex and on the species formed throughout the reaction.

1. Introduction

3,7-Diazabicyclo[3.3.1]nonanes, commonly known as bispidines, are heterocyclic compounds comprised by two condensed piperidine cores [1], existing in any of the three conformations showed in Figure 1 [2]. The chair-chair (**cc**) conformation, with a slight ring flattening, is generally favored [3], both in solution and in the solid state, as confirmed by X-ray studies on previous derivatives [4–6].

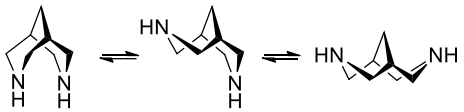

Figure 1. The unsubstituted bispidine nucleus and its three possible conformations: chair-chair (**cc**), chair-boat (**cb**), and boat-boat (**bb**).

Bispidines have basic properties and, despite being diamines, they titrate as monoamines because the proton is coordinated to both the nitrogen atoms through an intramolecular hydrogen bond that leads them to carry a partial positive charge [7]. These peculiar structures can coordinate several metal ions; the resulting complexes have unique, interesting properties, including the possibility to afford isomers with different geometries, which influence their chelating potential [8]. Although the bispidine fragment is quite rigid, its complex with a metal ion tolerates large differences in metal-donor distances, and thus it is not size-selective [9].

Among cations, zinc is one of the most biologically relevant, being the second most abundant transition metal in the human body. Zinc is essential for growth and development, and, at the cellular level, is critically involved in proliferation, differentiation, and apoptosis [10]. It is implicated in the regulation of cell metabolism and has catalytic, structural, and regulatory roles in more than two hundred metalloenzymes [11]. Several transcription factors have been found to possess a zinc-containing motif, serving as a DNA binder [12]. Many zinc complexes endowed with pharmacological properties were reported [13,14] in the field of antibacterial, antidiabetic, anti-inflammatory, and anti-Alzheimer drugs. Notably, zinc is significantly non-toxic compared to other metals, even at higher doses.

The nitrogen atoms in bispidines are almost ideally arranged for chelating metals, generating an adamantane-like structure, which leads to a rigid coordination and rather strong donor-ligand interactions [4]. Importantly, the substitution at the bridging 9-position of the bispidine ligand provides a means to alter the properties of the complexes without further enlarging the steric hindrance [4]. Besides their well-established use in the field of catalysis, these unique structures have also captured the attention of the pharmaceutical community over the years. Recently, bispidines have been studied as ligands for radiopharmaceutical applications [15], but also as diagnostic and therapeutic agents for cancer [16,17].

Based on these premises, we report the synthesis of the diol-bispidine derivative (3,7-bis(2-hydroxyethyl)-1,5-diphenyl-3,7-diazabicyclo[3.3.1]nonan-9-one), **1**, and its corresponding Zn(II) dinitrate complex $[Zn(C_{23}H_{26}N_2O_3)](NO_3)_2$, **2**, in order to lay the foundation for the future development of novel metal-based pharmaceuticals containing a bispidine core. The new compounds were synthesized and characterized following literature procedures [4]. In addition, to derive further information about the complexation mechanism and the conformational features, NMR titration experiments were performed, and the three-dimensional structure of the Zn(II) complex was determined by means of single-crystal X-ray diffraction (SC-XRD). Then, the free ligand and the Zn(II) complex were investigated by *ab initio* computational methods, using the density functional theory (DFT). This extensive structural investigation allowed us to determine whether the presence of substituent groups could lead to conformational changes in the bicyclic system, influencing the overall stability and complexation ability of the ligand.

2. Experimental

2.1 Synthesis

All reagents and solvents were purchased from commercial sources and used without further purification. The reactions were carried out in atmospheric conditions unless otherwise indicated. Reactions were monitored by thin-layer chromatography (TLC), performed on Merck Kieselgel 60 F254 plates. Visualization was accomplished by UV irradiation at 254 nm and, subsequently, by treatment with alkaline $KMnO_4$ (an oxidant mixture of $KMnO_4$, K_2CO_3, and 5% NaOH in water). ^1H and ^{13}C NMR spectra were recorded on a Bruker 400 spectrometer (^1H NMR, 400 MHz; ^{13}C NMR, 100 MHz), at room temperature, using tetramethylsilane (TMS, δ = 0.0 ppm) as internal standard. $CDCl_3$, CD_3CN, or CD_3OD were employed as solvents. Chemical shifts are reported as δ values in parts per million (ppm) from the internal standard; the coupling constants *J* are reported in Hz.

Synthesis of 3,7-bis(2-hydroxyethyl)-1,5-diphenyl-3,7-diazabicyclo[3.3.1]nonan-9-one (1). To an ice-cold solution of ethanolamine (1 eq.) in MeOH, neutralized by the slow addition of 3 mL of glacial acetic acid, was added formaldehyde (2 eq.) and 1,3-biphenyl propan-2-one (0-5 eq.). The resulting suspension was heated at 90 °C under reflux for 5 h and then cooled overnight. The solution was basified by the addition of a 20% NaOH solution; the dilution with an equal volume of water prompted the crystallization of the desired ligand A (Scheme 1). Yield: 68%. ^1H NMR (400 MHz, $CDCl_3$) δ 7.40 – 7.17 (m, 10H), 3.74 (t, *J* = 5.2 Hz, 4H), 3.66 (d, *J* = 11.2 Hz, 4H), 3.23 (d, *J* = 11.2 Hz, 4H), 2.74 (t, *J* = 5.2 Hz, 4H).

Synthesis of [3,7-bis(2-hydroxyethyl)-1,5-diphenyl-3,7-diazabicyclo[3.3.1]nonan-9-one]zinc(II) dinitrate (2). The ligand 1 (100 mg, 0.26 mmol) and $Zn(NO_3)_2{\cdot}6H_2O$ (77.3 mg, 0.26 mmol) were dissolved in 5 mL of acetonitrile. The solution was heated at 60 °C for 5 h and cooled down to room temperature. The mixture was evaporated under reduced pressure, affording a solid. ^1H NMR (400 MHz, $CDCl_3$) δ 7.50 – 7.17 (m, 10H), 4.31 (d, *J* = 12.0 Hz, 4H), 4.05 (m, *J* = 5.7 Hz, 4H), 3.21 (d, *J* = 11.9 Hz, 4H), 2.94 (m, 4H).

2.2 Crystallography

Diffraction data for **2** were collected on a Bruker Apex II CCD three-circle diffractometer, working at room temperature with graphite-monochromatized Mo-Kα X-radiation (λ = 0.71073 Å).

X-ray diffraction data in the θ range 2-25° were collected acquiring four sets of 360 bidimensional CCD frames with the following operative conditions: omega rotation axis, scan width 0.5°, acquisition time 50 s, sample-to-detector distance 50 mm, phi angle fixed at four different values (0°, 90°, 180° and 270°) for the four different sets.

Omega-rotation frames were processed with the *SAINT* software [18] for data reduction (including intensity integration, background, Lorentz, and polarization corrections) and for the determination of accurate unit-cell dimensions, obtained by least-squares refinement of the positions of 3571 independent reflections with I > 10σ(I). Absorption effects were empirically evaluated by the *SADABS* software [19] and absorption correction was applied to the data. The structure was solved by direct methods with *SIR-2014* [20] and completed by iterative cycles of full-matrix least squares refinement on F_o^2 and ΔF synthesis using *SHELXL-2018/3* [21] in the *WinGX v2021.3* suite [22]. Hydrogen atoms bonded to carbons were included at geometrically calculated positions and refined using a riding model. Uiso(H) were defined as 1·2Ueq of the parent carbon atoms for phenyl and methylene residues. The structure was analyzed with *PARST* [23],

Mercury 2021.3 [24], *ToposPro* [25], and *CrystalExplorer21* [26]. Graphical representations were generated with *ORTEP-3 2020.1* [22], *Mercury*, *ToposPro*, and *CrystalExplorer21*.

Crystal data for **2**: $C_{23}H_{26}N_4O_9Zn$, M_r = 567.85g/mol, Monoclinic, Space group $P2_1/c$, a = 9.4755(2) Å, b = 13.5820(3) Å, c = 19.2826(4) Å, β = 99.624(3), V = 2447(1) Å^3, Z = 4, D_{calc} = 1.542 Mg/m^3, F(000) = 1184, R = 0.0938 (for 2427 $F_o > 4sig(F_o)$), *wR2* = 0.1636, T = 294(2) K, *GOF* = 1.129. The reflections were collected in the range 1.84° ≤ θ ≤ 21.96° (limiting indices = -9 ≤ h ≤ 9, -14 ≤ k ≤ 14, -20 ≤ l ≤ 20) employing a 0.035 x 0.04 x 0.07 mm crystal. The residual positive and negative electron densities in the final map were 0.720 and -0.458 eÅ^{-3}.

2.3 Computational studies

Conformational analysis was performed with the software *Spartan '08* [27] by means of the "conformer distribution" function, using the Monte-Carlo search method. The MMFF force field *in vacuo* was used for the energy minimization of the structures, which were then submitted to a DFT single point energy calculation at the B3LYP 6-31G (d) level *in vacuo* with the software *Gaussian '09* [28]. All energies were corrected by adding the ZPE (Zero-point Energy), as obtained by frequency calculation at the same level.

3. Results and discussion

3.1 Synthetic procedures

The synthesis of the bispidine moiety is straightforward and allows the preparation of structurally diverse ligands [4]. The symmetrical bispidine **1** was prepared through a one-pot quadruple Mannich reaction, starting from 1,3-diphenyl acetone, four equivalents of formaldehyde, and two equivalents of ethanolamine (Scheme 1).

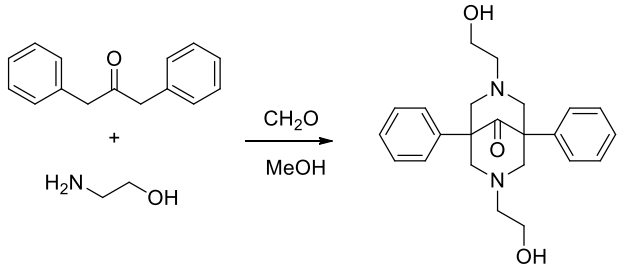

1

Scheme 1. Synthesis of ligand **1**.

The synthesized bispidine **1** was reacted with zinc nitrate hexahydrate to form the stable Zn(II) complex **2**. The metal center was found to be chelated by the nitrogen atoms of the heterocyclic core, by the two oxygens of the ethanol moieties, and by a nitrate group.

3.2 Crystallography

Crystals of **2**, suitable for X-ray diffraction analysis, were obtained as white plates from a 2:1 $CHCl_3$/MeOH solution. The ORTEP [22] drawing of the asymmetric unit (Figure 2), comprising the zinc complex and two nitrate anions, shows the coordination geometry around the metal center and the conformation of the ligand after the metal complexation.

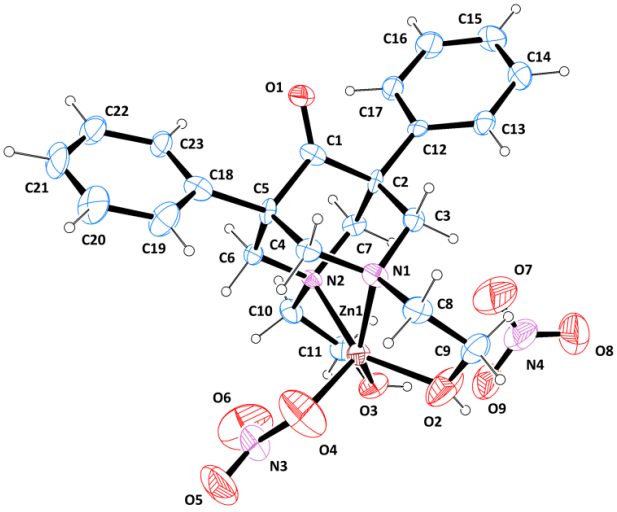

Figure 2. ORTEP view of **2** showing the arbitrary atom numbering (ellipsoids are at 40% probability and H atoms are represented as spheres of arbitrary radii).

Compound **2** crystallized in the monoclinic system, in the centrosymmetric space group $P2_1/c$. In this complex, the Zn(II) center is penta-coordinated by two nitrogen atoms from the bispidine core, two oxygen atoms from the chelating ethanolamine chains, and one oxygen atom from one of the nitrate anions. The corresponding values of distances and angles agree with literature data [29]. The coordination sphere around the cation can be described as a distorted square pyramid (Figure 3), the planar base being formed by N1, N2, O2, and O3 [maximum deviation from the mean plane: 0.003(6) Å, for O3], with the metal ion at 0.571(7) Å from this plane towards the apical site. The latter is occupied by one of the oxygen atoms of the nitro group (O4); its bond to zinc [Zn1···O4 of 2.048(8) Å] is tilted by about 22° with respect to the base normal.

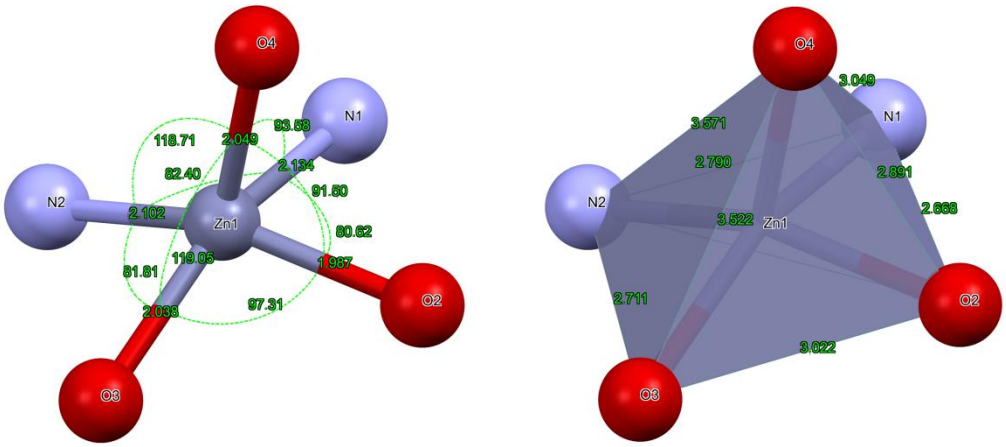

Figure 3. Coordination sphere of **2**: main distances and angles.

The geometry of the complex was also investigated by calculating the τ_5 value [30], which is defined as follows:

$$\tau_5 = \frac{\beta - \alpha}{60°}$$

where β > α, and β and α are the two greatest valence angles of the coordination center. The τ_5 value calculated for the complex is 0.006, indicating a square pyramidal shape.

The coordination topology was further examined by means of the Voronoi-Dirichlet tessellation of the space around the metal center [31,32]. The Voronoi-Dirichlet polyhedron (VDP) of an atom A surrounded by atoms X is a convex polyhedron, containing this atom, and delimited by perpendicular planes passing through the middle points of the segments A–X, connecting atom A with all other atoms X [33]. This approach has been used for ages to unambiguously determine the coordination number (CN) of metal crystals [34]. In detail, according to the Frank-Kasper definition of atomic domain, the CN is related to the number of faces of the enclosing VDP. More precisely, each neighboring atom contributes an amount proportional to the solid angle (SA) subtended by the corresponding face at the center of the VDP; hence, only the largest solid angles contribute to a unity of the CN [34]. In the present case, Zn1 is coordinated by N1, N2, O2, O3, O4: this is confirmed by the interatomic distances and by the SA (Table 1; Figure 4). All other neighboring atoms are characterized by very low SA and longer distances. Hence, these data unequivocally corroborate the fact that the Zn atom is penta-coordinated (CN = 5).

Table 1. Details of the VDP generated around the Zn atom, as calculated by *ToposPro* [25]. Only the distances (D) and solid angles (SA) of the coordinating atoms are shown.

Atom	D (Å)	SA (°)
N1	2.134(1)	14.28(8)
N2	2.101(6)	15.09(9)
O2	1.987(2)	17.06(3)
O3	2.038(2)	17.76(3)
O4	2.048(9)	17.44(9)
CN	5	
Rsd (Å)	1.351(0)	
V (Å^3)	10.329(4)	

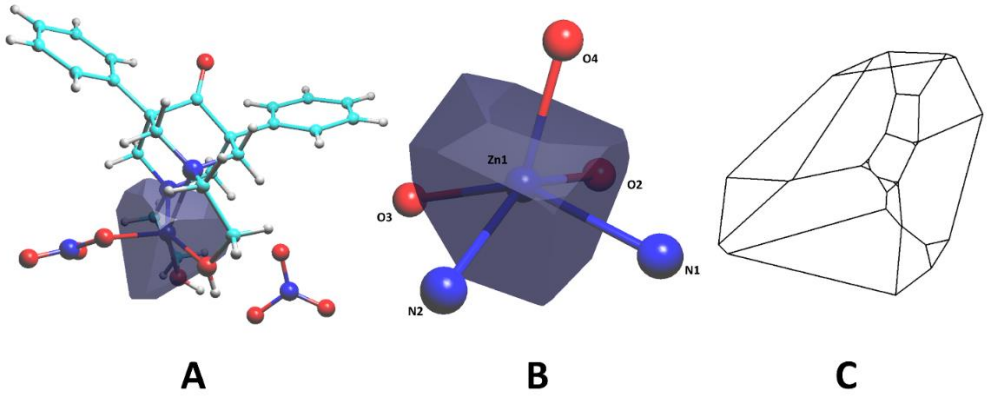

Figure 4. A. VDP calculated for the Zn metal center in complex **2**. **B.** Magnified view of the VDP calculated for the Zn atom. **C.** Schlegel projection of the VDP.

The bicyclo[3.3.1]nonane system adopts a **cc** conformation, and its puckering parameters are as follows: the C1/C2/C3/N1/C4/C5 heterocycle: Q_T = 0.608(3) Å and ϑ = 8.6(2)°, the C1/C5/C6/N2/C7/C2 piperidine ring: Q_T = 0.572(1) Å and ϑ = 3.6(9)°, indicating an almost perfect chair conformation for both rings. The two phenyls are oriented at 35(1)° with respect to each other.

The internal organization of the crystal is based on the repetition of units formed by two molecules of the complex, interacting through the free nitrate group, as depicted in Figure 5. In detail, strong H-bonds are established between the O9 oxygen of the anion and the hydroxyl groups of the bispidine side chains of two adjacent molecules. The phenyl groups of nearby complexes interact very weakly (Figure S1). In detail, the C18-C23 ring makes a T-shaped C-H···π interaction with the C12-C17 phenyl (centroid-centroid distance = 4.87(5) Å, angle between ring normals = 82.9(2)°). The latter and the corresponding ring of an adjacent complex lie on parallel planes at 2.85(2) Å. However, the centroid-centroid distance (5.12(8) Å) and the inclination of the centroid-centroid vector with respect to the plane normal (50.1(6)°) are incompatible with any significant form of stacking interaction.

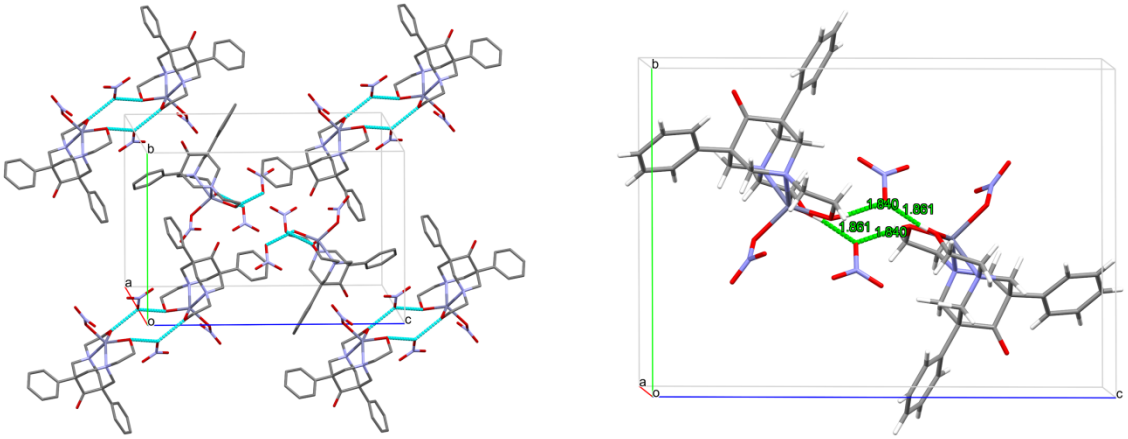

Figure 5. Crystal packing (left) and intermolecular interactions (right) of **2**, viewed along *a* axis.

3.3 Hirshfeld surface (HS) analysis

HS analysis and fingerprint plots, here generated with *CrystalExplorer21* [26,35], aided the examination of the intermolecular interactions in the crystal structure (Figure 6). The HS of **2** (V = 603.30 Å^3; A = 464.59 Å^2; G = 0.743; Ω = 0.069) was mapped over the normalized contact distance (d_{norm}), according to the following equation:

$$d_{norm} = \frac{d_i - r_i^{vdW}}{r_i^{vdW}} + \frac{d_e - r_e^{vdW}}{r_e^{vdW}}$$

where d_i is the distance between the HS and the nearest nucleus inside the surface, d_e is the distance between the HS and the nearest nucleus outside the surface, and r^{vdW} represents the van der Waals radius of the atom. The d_{norm} property was visualized with a red-blue-white color scheme, based on the length of the intermolecular contact with respect to the sum of the van der Waals radii (Figure 6A). The analysis of d_{norm} showed the presence of large red areas corresponding to the strong H-bonds established by the nitrate ion with the hydroxyl groups of the bispidine nucleus. Fainter red spots indicated the presence of weak H-bonds between O6 of the nitrate anion coordinating the metal center and two aromatic CH belonging to the two phenyl groups. The 2D fingerprint plots (Figure 6D), providing a visual summary of

the contribution of each contact type and the relative area of the surface corresponding to it, revealed the importance of the O···H/H···O contacts, which constitute 39.8% of the HS. The long spikes protruding towards the lower left corner of the graph confirmed the strong and short-range character of these interactions. The second and third contributors are H···H and C···H/H···C contacts, which make up 38.8% and 16.6% of the HS, respectively. The former represents non-specific van der Waals interactions, while the latter, constituting the wings of the plot, are mainly due to CH···π contacts. The lack of C···C interactions indicated the absence of parallel π-π stacking interactions; this observation was confirmed by the lack of the characteristic blue-red triangle pattern on the shape index (Figure 6B). The curvedness mapped over the HS showed the presence of flat areas, corresponding to the phenyl rings (Figure 6C).

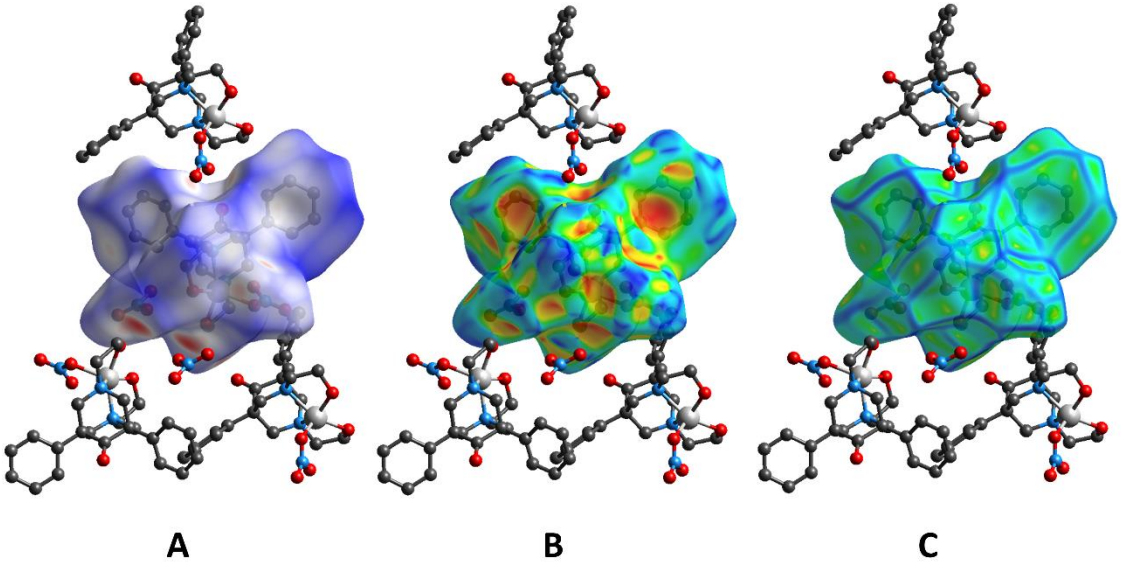

Figure 6. A. HS of **2** mapped over d_{norm} with a fixed color scale in the range -0.7408 au (red) – 1.5730 au (blue). Red, blue, and white indicate intermolecular contacts shorter, longer, and approximately equal to the sum of their van der Waals radii, respectively. **B.** HS of **2** mapped over the shape-index (color scale: -0.9975 au – 0.9990 au). Blue areas represent bumps and red regions indicate hollows. **C.** HS of **2** mapped over the curvedness (color scale: -3.7541 au – 0.2484 au). Green represents flat regions and blue indicates edges. [Continued]

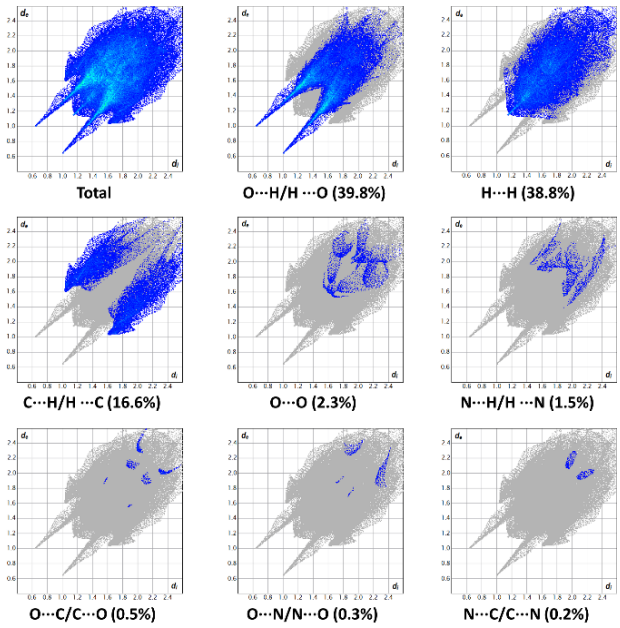

Figure 6. D. 2D Fingerprint plots of **2**, providing a visual summary of the frequency of each combination of d_e and d_i across the HS. Points with a contribution to the surface are colored blue for a small contribution to green for a great contribution.

The analysis of the intermolecular contacts on the HS of **2** according to Jelsch *et al.* [36] is reported in Table 2. In the first part, the surface contribution S_X of each chemical type *X* to the HS is indicated. The second part shows the proportions of the actual contacts (C_{XY}), and the third part the enrichment ratios (E_{XY}) of the various contact types. The reciprocal contacts X···Y and Y···X are merged and E_{XY} were not computed when the random contacts (R_{XY}) were lower than 0.9%. The E_{XY} ratios larger than unity indicate enriched contacts (in bold), while those lower than unity are impoverished. The percentages of actual contacts were calculated using *CrystalExplorer21* [26]. The same calculations were also performed for the ligand; details are reported in the Supplementary Materials (Table S1).

Table 2. Analysis of the intermolecular contacts on the HS of **2**.

Atoms	**H**	**C**	**N**	**O**	**Zn**
Surface (%)	67.8	8.7	1.0	22.6	0.0
Contacts (%)					
H	38.8				
C	16.6	0.0			
N	1.5	0.2	0.0		
O	39.8	0.5	0.3	2.3	
Zn	0.0	0.0	0.0	0.0	0.0
Enrichments					
H	0.8				
C	**1.4**	–			
N	**1.1**	–	–		
O	**1.3**	0.1	–	0.5	
Zn	–	–	–	–	–

3.4 NMR spectroscopy

The coordination chemistry of ligand **1** was investigated by ^{1}H NMR titration studies to gather information on the possible complexes formed in solution. ^{1}H NMR spectra of the free ligand in different solvents ($CDCl_3$, CD_3CN, and CD_3OD) were recorded. No significant differences in the chemical shifts were observed, and $CDCl_3$ was selected for further studies. The ligand was dissolved in $CDCl_3$ to a 0.01 mM concentration and then titrated with a CD_3OD solution of zinc nitrate hexahydrate, starting from 0.25 eq. up to 2 eq. of metal. During the addition of zinc nitrate to ligand **1**, we observed the formation of a new single species. After the addition of 1 eq. of metal, the free ligand completely disappeared, and only the new species was present, which was confirmed to be the expected complex **2** by comparing its spectrum to the one obtained by synthesis (Figure 7). In the complex, most of the NMR signals moved downfield with respect to the free ligand because of the deshielding effect of the metal cation. All the bispidine hydrogens were shifted, as well as the hydrogen atoms adjacent to the hydroxyl groups coordinating the metal. The most affected atoms were the equatorial hydrogens of the bispidine core ($\Delta\delta$ = 0.65 ppm) and the -CH_2O- hydrogens of the ethanol moiety ($\Delta\delta$ = 0.32 ppm).

The simultaneous decrease in intensity of the peaks of the free ligand, with only small changes in the chemical shifts, and the increase of the ones belonging to the complex indicated a moderately tight binding condition, resulting in a quite slow exchange process, in which two defined species are observed, the free ligand and the 1:1 metal/ligand complex. In the titration binding study, four different proton resonances associated with the observed changes in the chemical shifts were monitored, providing data from which the association constant (K_a) was determined by a global fitting analysis to a 1:1 binding model using the *supramolecular.org* web applet. The binding constant was calculated to be $1.26 \pm 0.16 \times 10^{7}$ M. The corresponding log K = 7.1 is comparable to previously reported log K values for tetracoordinated bispidine-zinc complexes [8].

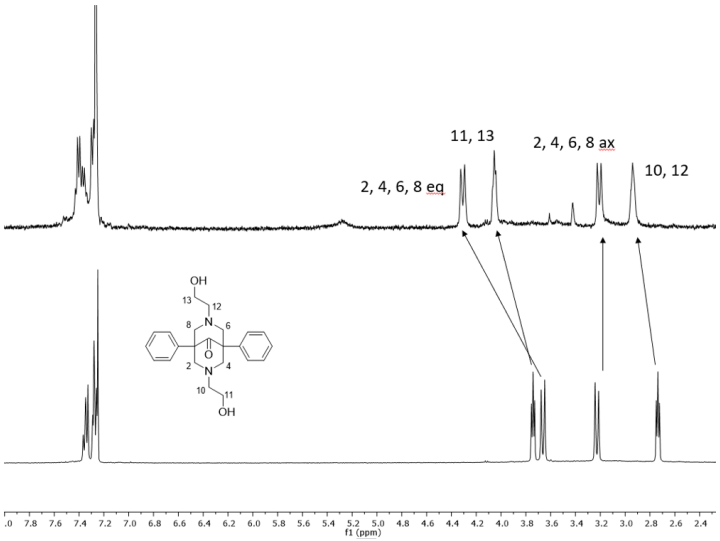

Figure 7. ^{1}H-NMR spectra of compounds **1** (bottom) and **2** (top).

3.5 Computational studies

To gather insights into the behaviour of the ligand, we investigated its structural features by computational tools (Monte Carlo search with Molecular Mechanic energy minimization - MC/MM: only

the conformers within 10 kcal/mol were considered). After the conformational analysis, the most favourable conformers were submitted to DFT-B3LYP/6-31G(d) energy optimization *in vacuo*. After frequency calculation, the energies were corrected by ZPE addition. 59 conformers were obtained from the conformational search. The minimum energy structure was in the **cc** conformation (only 11% of the structures were in the **cb** conformation).

After DFT optimization, the **cb** conformer was found to be 2.33 kcal/mol higher in energy compared to the **cc** conformer (Figure 8). This result agrees with the spectroscopic data, which showed half a set of signals, indicating that a single symmetric species, ascribed to the **cc** conformer, was present.

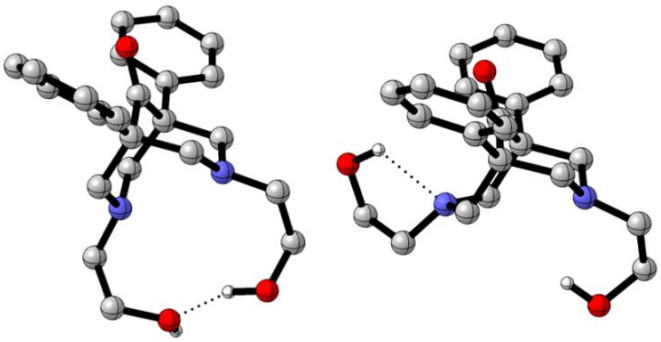

Figure 8. Plot of the lowest energy conformers for **1** as obtained from DFT calculations: **cc** conformation (left) and **cb** conformation (right).

The structure of the zinc complex was then optimized by DFT (Figure 9A). The most stable structure showed the presence of a single nitrate anion bound to a pentacoordinated Zn(II) cation at the center of a slightly distorted square-based pyramid geometry. The basis was formed by the two bispidine nitrogens and the two oxygen atoms of the ethanolic residue. The O-N-N-O dihedral had a value of 19.1°. The other parameters, bond lengths and angles, around the central Zn(II) atom were consistent with the results obtained from the solid-state X-ray diffraction analysis. As evidenced by the superimposition of the calculated and experimental structures (Figure 9B), only small differences in the position of the nitrate group coordinating the Zn(II) center were observed, thus confirming that the geometry in the solid state is not significantly affected by the crystal packing.

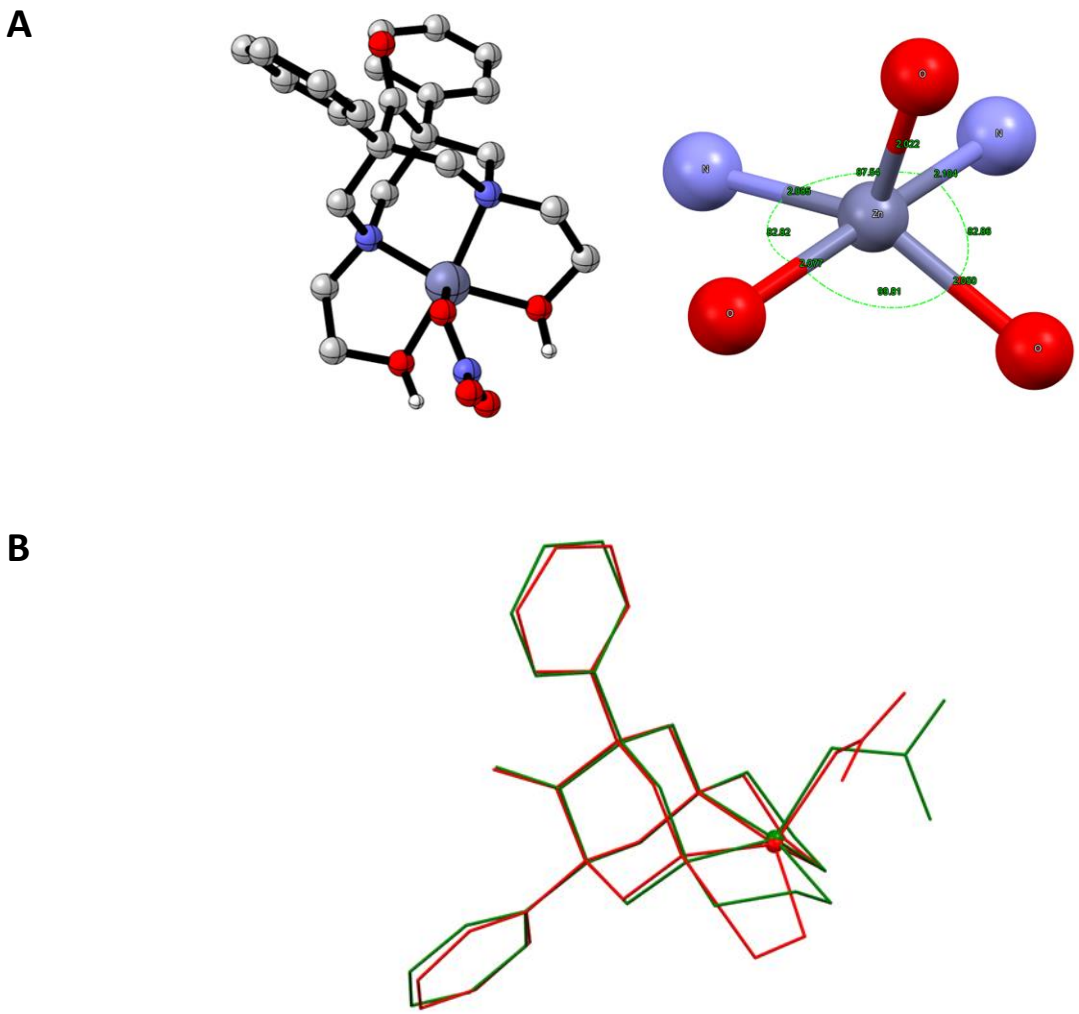

Figure 9. A. Plot of the lowest energy structure of **2** and its coordination sphere as obtained from DFT calculations. **B**. Overlay of the calculated (green) and experimental (red) structures.

Finally, the pharmacological and toxicological properties of compounds **1** and **2** were estimated by using the *DataWarrior* software [37] to gather preliminary information on their therapeutic potential. Because complexes often show different bioactivities compared to metal-free ligands, [16] the same parameters were calculated for both **1** and **2**. *DataWarrior* predicts toxicity risks by finding structural alerts within the test compound and computes a druglikeness score. A similar evaluation was also carried out using the *SwissADME* utility [38]. This online software also calculates whether the test sample is a pan-assay interference compound (PAIN). Similar filters are available also through the *SmartsFilter* [http://pasilla.health.unm.edu/tomcat/biocomp/smartsfilter] and *Zinc15 Patterns* [https://zinc15.docking.org/patterns/home/] services [39]. Overall, these approaches indicated that **1** and **2** exhibit desirable characteristics in terms of druggability and safety; moreover, the compounds successfully passed all the PAINS filters of the employed programs. In detail, **1** and **2** proved to be non-toxic, non-carcinogenic, non-mutagenic, and characterized by a high gastrointestinal absorption. Furthermore, they satisfied all criteria of the most common druglikeness indicators, including the Lipinski's rule of five. Therefore, the predicted pharmacological properties confirm that these compounds may be

considered as promising candidates for further biological studies. All calculations are reported in Table S2 and Table S3 (Supplementary Materials).

4. Conclusions

Bispidines are unique structures characterized by a natural tendency to chelate metal ions. The introduction of substituents and the variation of the metal center allows for the tailoring of their physico-chemical and biological properties. As a result, bispidines and their complexes can be adapted to serve many different purposes, spanning from the chemical catalysis to the pharmaceutical field. Because of the wide spectrum of their potential applications, the study of their three-dimensional structure and the comprehension of their mechanism of complexation continues to attract the interest of the scientific community. In this work, we synthesized and characterized a new bispidine ligand and its complex with Zn(II). The single-crystal X-ray analysis was pivotal to define the conformation of the bispidine core (**cc**) and to determine the geometry of the coordination sphere around the metal center (distorted square pyramid). The good agreement between the calculated and the experimental structure evidenced that the packing forces slightly influence the geometry of the complex, underlining the suitability of the ligand to provide a stable coordination. Finally, the NMR titration studies allowed us to follow the formation of the complex in solution and identify the correct stoichiometry. Overall, our investigations contribute to provide relevant information for the future development of bispidine derivatives into advanced candidates for a variety of different purposes, with a particular emphasis on pharmaceutical applications.

Supplementary data

Supplementary data are available at:

CCDC-2077338 number contains the supplementary crystallographic data for this paper. These data can be obtained free of charge *via* www.ccdc.cam.ac.uk/conts/retrieving.html (or from the Cambridge Crystallographic Data Centre, 12, Union Road, Cambridge CB21EZ, UK; fax: ++44 1223 336 033; or deposit@ccdc.cam.ac.uk).

Author Contributions

Matteo Mori: Investigation, writing - original draft, review & editing. Edoardo Fumagalli, Andrea Tresoldi: Investigation. Carlo Castellano: Investigation, Review & editing. Alessandro Sacchetti: conceptualization, review & editing. Fiorella Meneghetti: conceptualization, investigation, writing - original draft, review & editing.

Conflicts of interest

The authors declare that they have no known competing financial interests or personal relationships that could influence the work reported in this paper.

Acknowledgements

We acknowledge the University of Milan and the Polytechnic University of Milan for financial support.

References

[1] P. Parthiban, S. Kabilan, V. Ramkumar, Y.T. Jeong, Stereocontrolled facile synthesis and

antimicrobial activity of oximes and oxime ethers of diversely substituted bispidines, Bioorg. Med. Chem. Lett. 20 (2010) 6452–6458. https://doi.org/10.1016/J.BMCL.2010.09.079.

[2] R. Jeyaraman, S. Avila, Chemistry of 3-azabicyclo[3.3.1]nonanes, Chem. Rev. 81 (1981) 149–174. https://doi.org/10.1021/CR00042A002.

[3] G. Eglinton, J. Martin, W. Parker, 218. Bridged ring systems. Part V. Structural assignments in the bicyclo[3,3,1]nonane system by infrared spectroscopy, J. Chem. Soc. (1965) 1243–1251. https://doi.org/10.1039/JR9650001243.

[4] A. Rossetti, S. Landoni, F. Meneghetti, C. Castellano, M. Mori, G. Colombo Dugoni, A. Sacchetti, Application of chiral bi- and tetra-dentate bispidine-derived ligands in the copper(ii)-catalyzed asymmetric Henry reaction, New J. Chem. 42 (2018) 12072–12081. https://doi.org/10.1039/C8NJ01930D.

[5] M. Lippi, J. Caputo, A. Famulari, A. Sacchetti, C. Castellano, F. Meneghetti, J. Martí-Rujas, M. Cametti, Combined structural and theoretical investigation on differently substituted bispidine ligands: predicting the properties of their corresponding coordination polymers, Dalt. Trans. 49 (2020) 5965–5973. https://doi.org/10.1039/D0DT00799D.

[6] C. Castellano, A. Sacchetti, F. Meneghetti, Spectroscopic, Structural, and Computational Characterization of Three Bispidinone Derivatives, as Ligands for Enantioselective Metal Catalyzed Reactions, Chirality. 28 (2016) 332–339. https://doi.org/10.1002/CHIR.22586.

[7] J.E. Douglass, T.B. Ratliff, Synthesis of some 3,7-dialkyl-3,7-diazabicyclo[3.3.1]nonanes and a study of their conformations, J. Org. Chem. 33 (1968) 355–359. https://doi.org/10.1021/JO01265A073.

[8] K. Born, P. Comba, R. Ferrari, G.A. Lawrance, H. Wadepohl, Stability Constants: A New Twist in Transition Metal Bispidine Chemistry, Inorg. Chem. 46 (2007) 458–464. https://doi.org/10.1021/IC061501.

[9] C. Bleiholder, H. Börzel, P. Comba, R. Ferrari, M. Heydt, M. Kerscher, S. Kuwata, G. Laurenczy, G.A. Lawrance, A. Lienke, B. Martin, M. Merz, B. Nuber, H. Pritzkow, Coordination chemistry of a new rigid, hexadentate bispidine-based bis(amine)tetrakis(pyridine) ligand, Inorg. Chem. 44 (2005) 8145–8155. https://doi.org/10.1021/ic0513383.

[10] R.S. MacDonald, The Role of Zinc in Growth and Cell Proliferation, J. Nutr. 130 (2000) 1500S-1508S. https://doi.org/10.1093/JN/130.5.1500S.

[11] W. Maret, Regulation of Cellular Zinc Ions and Their Signaling Functions, in: Zinc Signal., Springer, Singapore, 2019: pp. 5–22. https://doi.org/10.1007/978-981-15-0557-7_2.

[12] D.J. Eide, Transcription factors and transporters in zinc homeostasis: lessons learned from fungi, Crit. Rev. Biochem. Mol. Biol. 55 (2020) 88–110. https://doi.org/10.1080/10409238.2020.1742092.

[13] K.D. Mjos, C. Orvig, Metallodrugs in Medicinal Inorganic Chemistry, Chem. Rev. 114 (2014) 4540–4563. https://doi.org/10.1021/CR400460S.

[14] Ł. Balewski, S. Szulta, A. Jalińska, A. Kornicka, A Mini-Review: Recent Advances in Coumarin-Metal Complexes With Biological Properties, Front. Chem. 9 (2021) 781779. https://doi.org/10.3389/FCHEM.2021.781779.

[15] N. Choudhary, A. Dimmling, X. Wang, L. Southcott, V. Radchenko, B.O. Patrick, P. Comba, C. Orvig, Octadentate oxine-armed bispidine ligand for radiopharmaceutical chemistry, Inorg. Chem. 58 (2019) 8685–8693. https://doi.org/10.1021/acs.inorgchem.9b01016.

[16] T. Price, S. Yap, R. Gillet, H. Savoie, L. Charbonniere, R. Boyle, A. Nonat, G. Stasiuk, T.W. Price, S.Y. Yap, L.J. Charbonnière, R.W. Boyle, A.M. Nonat, G.J. Stasiuk, Evaluation of a Bispidine-Based Chelator for Gallium-68 and of the Porphyrin Conjugate as PET/PDT Theranostic Agent, Chem. - A Eur. J. 26 (2020) 7602–7608. https://doi.org/10.1002/CHEM.201905776.

[17] H. Cui, R. Goddard, K.R. Pörschke, A. Hamacher, M.U. Kassack, Bispidine analogues of cisplatin, carboplatin, and oxaliplatin. Synthesis, structures, and cytotoxicity, Inorg. Chem. 53 (2014) 3371–3384. https://doi.org/10.1021/ic402737f.

[18] SAINT software reference manual, Bruker AXS, Madison, WI. 5465 (1998).

[19] S. Parkin, B. Moezzi, H. Hope, IUCr, XABS2: an empirical absorption correction program, J. Appl. Crystallogr. 28 (1995) 53–56. https://doi.org/10.1107/S0021889894009428.

[20] M.C. Burla, R. Caliandro, B. Carrozzini, G.L. Cascarano, C. Cuocci, C. Giacovazzo, M. Mallamo, A. Mazzone, G. Polidori, Crystal structure determination and refinement via SIR2014, J. Appl. Crystallogr. 48 (2015) 306–309. https://doi.org/10.1107/S1600576715001132.

[21] G.M. Sheldrick, Crystal structure refinement with SHELXL, Acta Crystallogr. Sect. C Struct. Chem. 71 (2015) 3–8. https://doi.org/10.1107/S2053229614024218.

[22] L.J. Farrugia, WinGX and ORTEP for Windows: an update, J. Appl. Crystallogr. 45 (2012) 849–854. https://doi.org/10.1107/S0021889812029111.

[23] M. Nardelli, PARST95 – an update to PARST: a system of Fortran routines for calculating molecular structure parameters from the results of crystal structure analyses, J. Appl. Crystallogr. 28 (1995) 659–659. https://doi.org/10.1107/S0021889895007138.

[24] C.F. MacRae, I. Sovago, S.J. Cottrell, P.T.A. Galek, P. McCabe, E. Pidcock, M. Platings, G.P. Shields, J.S. Stevens, M. Towler, P.A. Wood, Mercury 4.0: from visualization to analysis, design and prediction, J. Appl. Crystallogr. 53 (2020) 226–235. https://doi.org/10.1107/S1600576719014092.

[25] V.A. Blatov, A.P. Shevchenko, D.M. Proserpio, Applied topological analysis of crystal structures with the program package Topospro, Cryst. Growth Des. 14 (2014) 3576–3586. https://doi.org/10.1021/cg500498k.

[26] P.R. Spackman, M.J. Turner, J.J. McKinnon, S.K. Wolff, D.J. Grimwood, D. Jayatilaka, M.A. Spackman, CrystalExplorer: a program for Hirshfeld surface analysis, visualization and quantitative analysis of molecular crystals, J. Appl. Crystallogr. 54 (2021) 1006–1011. https://doi.org/10.1107/S1600576721002910.

[27] Y. Shao, L.F. Molnar, Y. Jung, J. Kussmann, C. Ochsenfeld, S.T. Brown, A.T.B. Gilbert, L. V. Slipchenko, S. V. Levchenko, D.P. O'Neill, R.A. DiStasio, R.C. Lochan, T. Wang, G.J.O. Beran, N.A. Besley, J.M. Herbert, C. Yeh Lin, T. Van Voorhis, S. Hung Chien, A. Sodt, R.P. Steele, V.A. Rassolov, P.E. Maslen, P.P. Korambath, R.D. Adamson, B. Austin, J. Baker, E.F.C. Byrd, H. Dachsel, R.J. Doerksen, A. Dreuw, B.D. Dunietz, A.D. Dutoi, T.R. Furlani, S.R. Gwaltney, A. Heyden, S. Hirata, C.P. Hsu, G. Kedziora, R.Z. Khalliulin, P. Klunzinger, A.M. Lee, M.S. Lee, W. Liang, I. Lotan, N. Nair, B. Peters, E.I. Proynov, P.A. Pieniazek, Y. Min Rhee, J. Ritchie, E. Rosta, C. David Sherrill, A.C. Simmonett, J.E. Subotnik, H. Lee Woodcock, W. Zhang, A.T. Bell, A.K. Chakraborty, D.M. Chipman, F.J. Keil, A. Warshel, W.J. Hehre, H.F. Schaefer, J. Kong, A.I. Krylov, P.M.W. Gill, M. Head-Gordon, Advances in methods and algorithms in a modern quantum chemistry program package, Phys. Chem. Chem. Phys. 8 (2006) 3172–3191. https://doi.org/10.1039/B517914A.

[28] M.J. Frisch, G.W. Trucks, H.B. Schlegel, G.E. Scuseria, M.A. Robb, J.R. Cheeseman, G. Scalmani, V. Barone, B. Mennucci, G.A. Petersson, H. Nakatsuji, M. Caricato, X. Li, H.P. Hratchian, A.F. Izmaylov, J. Bloino, G. Zheng, J.L. Sonnenberg, M. Hada, M. Ehara, K. Toyota, R. Fukuda, J. Hasegawa, M. Ishida, T. Nakajima, Y. Honda, O. Kitao, H. Nakai, T. Vreven, J.A. Montgomery, J.E. Peralta, F. Ogliaro, M. Bearpark, J.J. Heyd, E. Brothers, K.N. Kudin, V.N. Staroverov, R. Kobayashi, J. Normand, K. Raghavachari, A. Rendell, J.C. Burant, S.S. Iyengar, J. Tomasi, M. Cossi, N. Rega, J.M. Millam, M. Klene, J.E. Knox, J.B. Cross, V. Bakken, C. Adamo, J. Jaramillo, R. Gomperts, R.E. Stratmann, O. Yazyev, A.J. Austin, R. Cammi, C. Pomelli, J.W. Ochterski, R.L. Martin, K. Morokuma, V.G. Zakrzewski, G.A. Voth, P. Salvador, J.J. Dannenberg, S. Dapprich, A.D. Daniels, Ö. Farkas, J.B. Foresman, J. V Ortiz, J. Cioslowski, D.J. Fox, Gaussian 09 Revision A.2, (2009).

[29] M. Harvey, S. Baggio, R. Baggio, A.W. Mombrú, (Acetato-O,O')(acetato-O)(2,9-dimethyl-1,10-phenanthroline-N,N')zinc(II), Acta Crystallogr. Sect. C. 55 (1999) 308–310. https://doi.org/10.1107/S0108270198013481.

[30] A.W. Addison, T.N. Rao, J. Reedijk, J. Van Rijn, G.C. Verschoor, Synthesis, structure, and spectroscopic properties of copper(II) compounds containing nitrogen–sulphur donor ligands; the crystal and molecular structure of aqua[1,7-bis(N-methylbenzimidazol-2'-yl)-2,6-dithiaheptane]copper(II) perchlorate, J. Chem. Soc. Dalt. Trans. (1984) 1349–1356. https://doi.org/10.1039/DT9840001349.

[31] V.A. Blatov, A.P. Shevchenko, V.N. Serenzhkin, Crystal space analysis by means of Voronoi–Dirichlet polyhedra, Acta Crystallogr. Sect. A. 51 (1995) 909–916. https://doi.org/10.1107/S0108767395006799.

[32] V.A. Blatov, Voronoi–dirichlet polyhedra in crystal chemistry: theory and applications, Crystallogr. Rev. 10 (2007) 249–318. https://doi.org/10.1080/08893110412331323170.

[33] V.N. Serezhkin, A. V. Savchenkov, Application of the Method of Molecular Voronoi-Dirichlet Polyhedra for Analysis of Noncovalent Interactions in Aripiprazole Polymorphs, Cryst. Growth Des. 20 (2020) 1997–2003. https://doi.org/10.1021/acs.cgd.9b01645.

[34] M. O'Keeffe, IUCr, A proposed rigorous definition of coordination number, Acta Crystallogr. Sect. A. 35 (1979) 772–775. https://doi.org/10.1107/S0567739479001765.

[35] F.L. Hirshfeld, Bonded-atom fragments for describing molecular charge densities, Theor. Chim. Acta. 44 (1977) 129–138. https://doi.org/10.1007/BF00549096.

[36] C. Jelsch, K. Ejsmont, L. Huder, The enrichment ratio of atomic contacts in crystals, an indicator derived from the Hirshfeld surface analysis, IUCrJ. 1 (2014) 119–128. https://doi.org/10.1107/S2052252514003327.

[37] T. Sander, J. Freyss, M. Von Korff, C. Rufener, DataWarrior: An open-source program for chemistry aware data visualization and analysis, J. Chem. Inf. Model. 55 (2015) 460–473. https://doi.org/10.1021/ci500588j.

[38] A. Daina, O. Michielin, V. Zoete, SwissADME: a free web tool to evaluate pharmacokinetics, drug-likeness and medicinal chemistry friendliness of small molecules, Sci. Rep. 7 (2017) 1–13. https://doi.org/10.1038/srep42717.

[39] M. Mori, E. Gilardoni, L. Regazzoni, A. Pedretti, D. Colombo, G. Parkinson, A. Asai, F. Meneghetti, S. Villa, A. Gelain, Towards the Inhibition of Protein–Protein Interactions (PPIs) in STAT3: Insights into a New Class of Benzothiadiazole Derivatives, Molecules. 25 (2020) 3509. https://doi.org/10.3390/MOLECULES25153509.